Lensless ghost imaging with true thermal light

Xi-Hao Chen, Qian Liu, Kai-Hong Luo and Ling-An Wu

Laboratory of Optical Physics, Institute of Physics, Chinese Academy of Sciences, Beijing 100190, China

Compiled February 21, 2009

We report the first (to our knowledge) experimental demonstration of lensless ghost imaging with true thermal light. Although there is no magnification, the method is suitable for all wavelengths and so may find special applications in cases where it is not possible to use lenses, such as with x-rays or γ-rays. We also show numerically that some magnification may be realized away from the focal plane, but the image will always be somewhat blurred.

OCIS codes: 110.6820, 030.0030, 030.5260

Since the first "ghost" imaging experiment [1] based on quantum entangled photon pairs was performed, over the past decade the phenomenon has attracted much attention in the field of quantum optics. It is well-known now that ghost imaging, or correlated two-photon imaging, can be performed not only with entangled photon pairs but also with a classical thermal source. The difference between these two approaches has been widely discussed by the groups of Shih [2], Boyd [3], Lugiato [4], Zhu [5] and Wang [6]. More recently, theoretical and experimental studies [7–14] on lensless ghost imaging with thermal light have drawn new attention; here "lensless" means that no lens is used for imaging the object. The possibility to perform lensless ghost imaging with thermal light was first predicted by Wang and collaborators [6], who proposed in their paper that the thermal source behaves as a phase-conjugate mirror which reflects an object onto itself. The first experiment with a classical pseudothermal source that successfully demonstrated lensless ghost imaging was performed by Scarcelli et al. [8,9], which led to a debate [8–10, 14–16] on the question whether two-photon correlation phenomena must be described quantum mechanically, regardless of whether the light source is classical or quantum. Though there is still no consensus on the subject so far, this does not affect potential applications of ghost imaging with thermal light. In particular, the recent lensless ghost imaging experiments in which reflected and scattered light from the object were detected by second-order correlation measurements show good promise for practical applications. [11,12] However, in all the above experiments, the primary light source was pseudothermal radiation obtained by passing a laser beam through a rotating ground glass plate.

Different from these experiments and based on our previous work [17, 18] with true thermal radiation, we report the first demonstration of a lensless ghost imaging experiment using a true thermal light source. We employed a commercial rubidium hollow-cathode lamp (HCL) manufactured by the General Research Institute for Nonferrous Metals (China); however, this time the wavelength used was not the 780 nm of Rb as in our previous papers but the 692.9 nm line of neon, a buffer gas in the lamp. The coherence time τ_0 of the lamp powered by a direct current of 30 mA was estimated from a Hanbury Brown-Twiss (HBT) type measurement of the second-order correlation function [17, 19], and found to be about 0.1 ns. This is much shorter than that of experiments using pseudothermal radiation from a laser beam randomly scattered by a ground glass plate. An outline of the experimental setup is shown in Fig. 1. The light from the lamp is passed through a monochromator to select out the 692.9 nm spectral line, and is focused by the convex lens L_1 of 10 cm focal length to form a secondary light source, an image of the cathode about 1.67 mm in diameter. A polarizing beam splitter (PBS) transmits linearly polarized light. After reflection by mirror M the beam is divided by a 50:50 nonpolarizing beamsplitter (BS). The object, a mask O consisting of two pinholes of diameters 0.77 and 0.72 mm, 3.66 mm apart, is inserted into the beam transmitted through BS. The mask was made simply by pricking two holes in a piece of copper foil, with the result that the hole diameters were not exactly equal. Two lenses L_2 and L_3 act as a telescope, so that the single-photon detector

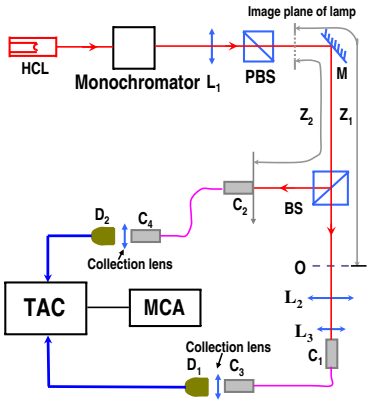

Fig. 1. (Color online) Lensless ghost imaging experimental setup. Object mask O is at a distance of $z_1 = z_2 =$ 170 cm from the image plane of the lamp cathode; D_1 is a bucket detector; C_2 is a fiber collimator scanned in the transverse direction and connected to detector D_2. See text for explanation of other elements.

D_1 (Perkin Elmer SPCM-AQR-12) can capture all the light passing through the mask by means of fiber collimators C_1, C_3 and a collection lens, thus serving as a bucket detector. The reflected light from BS is coupled into detector D_2 by fiber collimators C_2, C_4 and a collection lens. Note that the lenses merely serve the purpose of collecting light; in the paths from the effective plane of the lamp to the object and to fiber collimator C_2 (z_1 and z_2, respectively) there is no lens. The receiving area of the collimators is about 1.8 mm in diameter. The detector output signals are sent to a time-to-amplitude converter (TAC), with detectors D_1 and D_2 providing the "start" and "stop" signals, respectively. The TAC output is connected to a multi-channel analyzer (MCA), which displays a histogram of the coincidence counts as a function of the difference in the times of arrival of the photons at the two detectors.

The transverse normalized second-order correlation function is given by [2, 14]:

$$g^{(2)}(x_2) \propto N + |T(x_2)|^2, \tag{1}$$

where x_2 is the transverse position of fiber collimator C_2, $T(x)$ the transmission function of the mask, and N the number of transparent features in the object, which equals 2 in our scheme because the mask has two pinholes. This equation reflects the position-position correlation between the object and image planes, as well as the fact that the visibility decreases (background increases) when the number of points in the object increases.

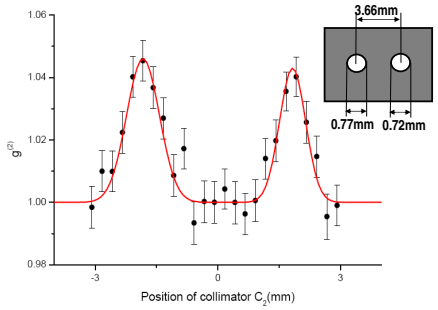

Fig. 2. (Color online) Dependence of $g^{(2)}(x_2)$ on the position of fiber collimator C_2, which gives the cross-sectional image of the mask. The solid curve is a Gaussian fit. Inset: object mask with two pinholes of diameters 0.77 and 0.72 mm, 3.66 mm apart.

In our experiment we choose the case in which the distance z_1 between the object and the effective plane of the lamp is equal to the distance z_2 between the plane of the lamp and the fiber collimator C_2, namely, $z_1 = z_2 = 170$ cm. The collimator C_2 is scanned transversely across the reference beam in steps of 0.25 mm, and the detector coincidence counts recorded. The normalized second-order correlation function $g^{(2)}(x_2)$ is calculated as previously [17, 18], from which we plot the cross-sectional image of the two-pinhole object, as shown in Fig. 2. The two peaks are not symmetrical, clearly reflecting the slight difference in size of the two pinholes, but it can be seen that there is no magnification of the image. The visibility is found to be 2.2%, which is lower than the value of 5% that we obtained in the HBT experiment. This is as expected, since different points on an object will diminish the visibility of the image of other points, so the more complicated the object, the worse will the visibility be. Apart from the factor N in expression (1), other reasons for the lower visibility include the short coherence time compared with the time jitter of the detection system, the limited transverse coherence area of about 0.5 mm^2 in the object plane, and the finite area of the fiber collimator C_2. The latter also lowers the resolution, which is, moreover, adversely affected when the coherence area is too large.

We know that, in the classical optics approximation, a lens generates an image of an object in the plane defined by the Gaussian thin-lens equation. Basically, this equation defines a point-to-point relationship between the object plane and image plane. However, in practice it is sometimes said that an image can also be obtained before and behind the focal plane, albeit at the price of blurring the image. We would then expect that this could also be said for second-order lens-focused ghost imaging with thermal light, and therefore, also be true for the lensless scheme, which is just a special case of having a lens of infinite focal length. It has been reported in Ref. [13] that the longitudinal coherence length of a thermal light source determines the region where the ghost image exists. This implies that an image can be obtained in any plane of this region, as in the above-mentioned case of classical first-order imaging. However, in the out-of-focus condition $z_1 \neq z_2$ there will never be a "perfect" image. This has been seen from the experimental results in Ref. [14], where a perfectly sharp image is only obtained in the focused condition $z_1 = z_2$ and the imaging quality becomes worse and worse with the increase of Δz ($= z_2 - z_1$), as in the classical case. Thus strictly speaking there is no magnification in lensless ghost imaging; an image in the focal plane has the same size as the object, while all images in the out-of-focus planes are blurred compared with that at the focus.

For a better understanding of lensless ghost imaging in the defocused case we perform a numerical simulation of an experiment. The experimental scheme is almost the same as in some of the papers mentioned above. With x_1 and x_2 representing the transverse coordinates in the planes of the bucket detector D_1 and the point detector D_2, the transverse normalized second-order intensity fluctuation correlation function is

$$\Delta g^{(2)}(x_2) = \int \frac{\langle \Delta I_1(x_1) \Delta I_2(x_2) \rangle}{\langle I_1(x_1) \rangle \langle I_2(x_2) \rangle} dx_1, \tag{2}$$

where $\Delta I_i(x_i)$ and $I_i(x_i)$ are the intensity fluctuation and intensity at the detector positions x_i ($i = 1, 2$), respectively. Thus we see that $\Delta g^{(2)}(x_2)$ depends on the second-order intensity fluctuation correlation

$\langle \Delta I_1(x_1)\Delta I_2(x_2)\rangle$, which can be expressed as

$$\langle \Delta I_1(x_1)\Delta I_2(x_2)\rangle \propto \left| \int h_2^*(x^{'},x_2)h_1(x^{'},x_1)dx^{'} \right|^2$$
$$\propto \left| \int \exp[\frac{\pi^2(x^{'}-x_1)^2(x^{'}-x_2)^2}{\lambda^2 z_1 z_2}]T(x_1)dx^{'} \right|^2, \quad (3)$$

in which

$$h_1(x,x_1) \quad \propto \quad \exp[\frac{i\pi(x-x_1)^2}{\lambda z_1}]T(x_1), \quad (4)$$

$$h_2(x,x_2) \quad \propto \quad \exp[\frac{i\pi(x-x_2)^2}{\lambda z_2}], \quad (5)$$

and $h_i(x,x_i)$ is the impulse response function for light propagating from a point x on the source to a point x_i in the detector plane, and z_1, z_2 are the respective distances from the source to the object and to the detector D_2.

In our simulation a light source of wavelength 693 nm and radius 6 mm and z_1=300 mm is chosen, and the object is a double-slit with slits of width 100 μm separated by 200 μm. The normalized second-order intensity fluctuation correlation function $\Delta g^{(2)}$ is plotted against x_2 and z_2 in Fig. 3. It can be clearly seen that both the visibility and the resolution of the image become worse and worse as z_2 deviates from the position $z_2 = z_1$, and a sharp image can only be obtained in the focused condition. Though we can obtain fairly clear images a short distance away, they are still blurred compared with that in the plane of focus. It is true that the images in the planes of $z_2 < z_1$ are broader than at the focus, but it would be rather factitious to say that this is actually magnification. It is also contradictory to say that the image magnification is z_2/z_1, as mentioned in [10] and [13], since in this case we have $z_2 < z_1$.

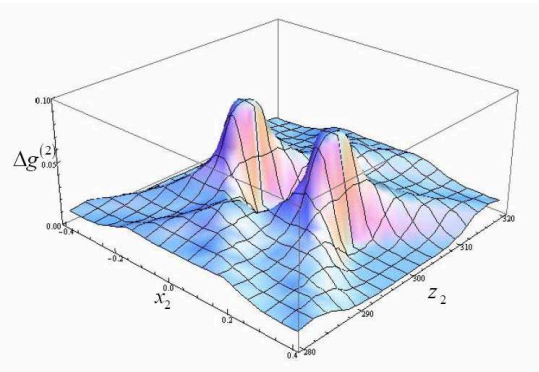

Fig. 3. (Color online) Numerical simulation of $\Delta g^{(2)}$ for lensless ghost imaging as a function of x_2 and z_2 in mm. The object is a double-slit of slit width 100 μm and separation 200 μm, at a distance of z_1=300 mm from a 693 nm thermal light source of radius 6 mm.

In conclusion, we have experimentally realized lensless ghost imaging with true thermal light. Although the original visibility is very low the reconstructed image may be clearly recognizable as the background can be easily removed by standard image processing techniques. Since the imaging setup works for any wavelength and no lenses are required, such a method seems quite promising for imaging applications at wavelengths such as x-rays or γ-rays where no effective lens is available. Thermal light sources are easier to obtain, and so it is conceivable that they could find certain special applications [20] where entangled or pseudo-thermal sources are not so convenient to use. We have also demonstrated theoretically that in thermal lensless ghost imaging a really sharp image can only be obtained at the focus, in which case there is no magnification. The image in all other planes even when within the longitudinal coherence length is always blurred compared to that in the focal plane.

This work was supported by the National Natural Science Foundation of China (Grants 60578029 and 10674174), and the National Program for Basic Research in China (Grant 2006CB921100). L. A. Wu's e-mail address is wula@aphy.iphy.ac.cn.

References

1. T. B. Pittman, Y. H. Shih, D. V. Strekalov, and A. V. Sergienko, Phys. Rev. A **52**, R3429 (1995).
2. A. Valencia, G. Scarcelli, Milena DAngelo, and Y. Shih, Phys. Rev. Lett. **94**, 063601 (2005).
3. R. S. Bennink, S. J. Bentley, R. W. Boyd, and J. C. Howell, Phys. Rev. Lett. **92**, 033601 (2004).
4. A. Gatti, E. Brambilla, M. Bache, and L. A. Lugiato, Phys. Rev. Lett. **93**, 093602 (2004).
5. Y. J. Cai and S. Y. Zhu, Phys. Rev. E, **71**, 056607 (2005).
6. D. Z. Cao, J. Xiong, and K. G. Wang, Phys. Rev. A **71**, 013801 (2005).
7. Y. J. Cai and F. Wang, Opt. Lett. **32**, 205 (2008).
8. G. Scarcelli, V. Berardi and Y. H. Shih, Appl. Phys. Lett. **88**, 061106 (2006).
9. G. Scarcelli, V. Berardi and Y. H. Shih, Phys. Rev. Lett. **96**, 063602 (2006).
10. L. Basano and P. Ottonelloa, Appl. Phys. Lett. **89**, 091109 (2006).
11. R. Meyers, K. S. Deacon, and Y.H. Shih, Phys. Rev. A **77**, 041801(R) (2008).
12. R. Meyers, K. S. Deacon, and Y.H. Shih, J. Mod. Opt. **54**, 2381(2007).
13. H. L. Liu and S. S. Han, Opt. Lett. **33**, 824 (2008).
14. F. Ferri, D. Magatti, V. G. Sala, and A. Gatti, Appl. Phys. Lett. **92**, 261109 (2008).
15. A. Gatti, M. Bondani, L. A. Lugiato, M. G. A. Paris, and C. Fabre, Phys. Rev. Lett. **98**, 039301 (2007).
16. G. Scarcelli, V. Berardi and Y. H. Shih, Phys. Rev. Lett. **98**, 039302 (2007).
17. D. Zhang, Y. H. Zhai, L. A. Wu and X. H. Chen, Opt. Lett. **30**, 2354 (2005).
18. Y. H. Zhai, X. H. Chen, D. Zhang, and L. A. Wu, Phys. Rev. A **72**, 043805 (2005).
19. R. Hanbury Brown, *The intensity interferometer*, (Taylor and Francis Ltd. London 1974), see Eq. 4.26.
20. J. Cheng and S. S. Han, Phys. Rev. Lett. **92**, 093903 (2004).